1984

NASA/ASEE SUMMER FACULTY RESEARCH FELLOWSHIP PROGRAM

MARSHALL SPACE FLIGHT CENTER

THE UNIVERSITY OF ALABAMA

SINGULAR ASYMPTOTIC EXPANSIONS IN NONLINEAR ROTORDYNAMICS

Prepared by: William B. Day, Ph.D.

Academic Rank: Associate Professor

University and Department: Auburn University

Department of Computer Science

NASA/MSFC

Laboratory: Systems Dynamics

Division: Control Systems

Branch: Servomechanisms & Systems Stability

NASA Counterpart: Luke A. Schutzenhofer, Ph.D.

Date: August 10, 1984

Contract No.: NASA-NGT-01-002-099

(The University of Alabama)

SINGULAR ASYMPTOTIC EXPANSIONS IN NONLINEAR ROTORDYNAMICS

BY

WILLIAM B. DAY, Ph.D.
ASSOCIATE PROFESSOR OF COMPUTER SCIENCE
AUBURN UNIVERISTY, ALABAMA

ABSTRACT

During hot firing ground testing of the Space Shuttle's Main Engine, vibrations of the liquid oxygen pump have occurred at frequencies which cannot be explained by the linear Jeffcott model of the rotor. The model becomes nonlinear after accounting for deadband, side forces, and rubbing. Two phenomena present in the numerical solutions of the differential equations are unexpected periodic orbits of the rotor and "tracking" of the nonlinear frequency. A multiple-scale asymptotic expansion of the differential equations is used to give an analytic explanation of these characteristics.

LIST OF FIGURES

1. Introduction:

Excessive vibrations of the liquid oxygen turbopump in the Space Shuttle's Main Engine have been recorded during hot firing ground testing. Examination of the power spectral density (PSD) plot reveal frequencies which cannot be explained using the linear rotordynamics model of Jeffcott [5]. Consequently, numerous investigations have been undertaken to study such rotors and to provide descriptions of the solution of the two, coupled, second-order differential equations which describe the motion of the rotor's center of mass. Following the early work in rotordynamics by Yomamoto [7], one introduces a nonlinearity to the Jeffcott equations by including the effect of bearing clearance or deadband. In the pump this deadband refers to the load carriers (ball bearings) and physically describes the clearance between the outer race of the bearing and the support housing. Both empirical results by Childs [1,2] and Gupta et al. [4] and numerical solutions using the fourth order Runge-Kutta algorithm by Control Dynamics Company [3] have been helpful in understanding the rotor's motion for the nonlinear problem. This report extends the earlier work by using analytic expressions obtained from singular asymptotic expansions (methods of multiple scales) to quantize the solution.

Section 2 presents the general analysis of a Jeffcott rotor with deadband and sinusoidal forcing. This discussion includes a derivation of the characteristic, nonlinear frequency which is responsible for "tracking", a shift in the subsynchronous frequency as a function of the external force. Then the method of multiple scales provides justification for inclusion or exclusion of the subsynchronous term in the solution expression.

Section 3 displays three examples. The first example illustrates the major theoretical devices of section 2. Example 2 uses data from CDC report [3] where the subsynchronous frequency begins at one-half the forcing frequency. It reiterates the mathematical development of section 2. The last example uses the data of example 1 to produce a frequency-response plot for the nonlinear problem. How this plot differs from the corresponding linear case and what one may expect in the general case are the major points

made in this example. All the examples use the method of Runge-Kutta to obtain numerical solutions.

Section 4 concludes the report with brief descriptions of extension and related problems. These include multiple external forces (e.g. sideforce), rubbing, asymmetric stiffness, and stability analysis.

2. General Theory:

The linear Jeffcott equations which describe the motion of a rotor in the inertial, Cartesian coordinate system are these:

$$(1.)\quad m\ddot{y}=-C_S\dot{y}-K_Sy-Q_Sz+mu\omega^2\cos\omega t$$

$$(2.)\quad m\ddot{z}=-C_S\dot{z}+Q_Sy-K_Sz+mu\omega^2\sin\omega t$$

where

m = mass (kg.)

C_S = seal damping (kg./s.)

K_S = seal stiffness (kg./s.^{2})

Q_S = cross-coupling stiffness of seal (kg./ s.^{2})

u = displacement of the shaft center of mass from the geometric center (m.)

ω = angular velocity of the shaft (rad./s.)

For the model to include bearing forces which hold the rotor in position, one adds the terms

$$-K_B(y-y\delta/\sqrt{y^2+z^2})+\mu K_B(z-z\delta/\sqrt{y^2+z^2})$$

and

$$-\mu K_B(y-y\delta/\sqrt{y^2+z^2})-K_B(z-z\delta/\sqrt{y^2+z^2}),$$

respectively, to the right-hand sides of equations (1.)

and (2.). Here K_B (kg./s.^{2}) is the bearing stiffness, δ (m.) is the clearance or deadband between the housing and the bearing, and μ (nondimensional) is the coefficient of friction between the housing and the bearing. These bearing forces occur only when $\sqrt{y^2+z^2}>\delta$; otherwise, they are zero. Equations (1.)-(2.) then become

$$(3.)\quad \ddot{y}+(C_S/m)\dot{y}+(1/m)[K_S+K_B(1-\delta/r)]y+(1/m)[Q_S-\mu K_B(1-\delta/r)]z = u\omega^2\cos\omega t$$

$$(4.)\quad \ddot{z}+(C_S/m)\dot{z}-(1/m)[Q_S-\mu K_B(1-\delta/r)]y+(1/m)[K_S+K_B(1-\delta/r)]z = u\omega^2\sin\omega t$$

when $r=\sqrt{y^2+z^2}>\delta$; otherwise, $K_B=0$.

Equations (3.)-(4.) can be put in nondimensional form using a displacement g and a frequency σ. Thus, using $Y=y/g$, $Z=z/g$, and $\tau=\sigma t$, the dimensionless equations are these:

$$(5.)\quad Y''+CY'+[A+k(1-\Delta/R]Y+[B-\mu k(1-\Delta/R)]Z=E\phi^2\cos\phi t$$

$$(6.)\quad Z''+CZ'-[B-\mu k(1-\Delta/R)]Y+[A+k(1-\Delta/R)]Z=E\phi^2\sin\phi\tau$$

where prime denotes differentiation with respect to τ and $C=C_S/m/\sigma$, $A=K_S/m/\sigma^2$, $k=K_B/m/\sigma^2$, $B=Q_S/m/\sigma^2$, $\Delta=\delta/g$, $R=r/g$, $E=u/g$, and $\phi=\omega/\sigma$.

Equations (5.)-(6.) can be reduced to the following single equation by defining $W=Y+iZ$:

$$(7.)\quad W''+CW'+\{A+k(1-\Delta/|W|)+i[-B+\mu k(1-\Delta/|W|)]\}W=E\phi^2\exp(i\phi\tau)$$

Furthermore, the polar form of equations (5.)-(6.) is

$$(8.)\quad R''+CR'+[A+k(1-\Delta/R)-(\Theta')^2]R=E\phi^2\cos(\phi\tau-\Theta)$$

$$(9.)\quad R\Theta''+(2R'+CR)\Theta'=R[B-\mu k(1-\Delta/R)]+E\phi^2\sin(\phi\tau-\Theta)$$

where $R=(Y^2+Z^2)^{1/2}$ and $\Theta=\text{Arctan}\ (Z/Y)$. Since μ is nondimensional and typically small, one may regard it as zero without affecting the qualitative results.

Consider the homogeneous (E=0) equation corresponding to equation (7.). If this equation were also linear ($\Delta=0$),

then exponentially growing or decaying solutions would result for a given set of system parameters. In the special case that $(B/C)^2=A+k$, a sinusoidal solution is obtained with frequency $\beta=B/C$. To see this, consider the characteristic equation for $W=\exp(m\tau)$:

$$m^2+Cm+[A+k-iB]=0$$

$$m=-C/2\pm\{C^2/4-A-k+iB\}^{1/2}$$

$$m=-C-iB/C,\ iB/C.$$

In the nonlinear, homogeneous problem, k is replaced by $k(1-\Delta/R)$; hence, if R is a constant, then there is a wide spectrum for which $(B/C)^2=A+k(1-\Delta/R)$; i.e., if

$$(10.)\quad A<(B/C)^2\leq A+k,$$

then there is a constant value of R (with $R>\Delta$) for which $(B/C)^2=A+k(1-\Delta/R)$. This value of R is denoted by a and the corresponding frequency by $\beta_0=B/C$. This frequency is labeled the characteristic, nonlinear frequency. Thus, whenever inequality (10.) is satisfied, equations (5.)-(6.) with E=0 have steady-state solutions $Y=a\cos(\beta_0\tau)$ and $Z=a\sin(\beta_0\tau)$.

The same results can be found from the polar equations (8.)-(9.) by assuming R and Θ' are constants. Then with E=0 those equations become

$$[A+k(1-\Delta/R)-(\Theta')^2]R=0,\qquad C\Theta'=B.$$

Thus, $\beta_0=\Theta'=B/C$ and $a=R=k\Delta/(A+k-\beta_0^2)$.

Notice that $\beta_0=B/C\leq A+k=\{(K_S+K_B)/m\}^{1/2}/\sigma=\omega_0$, the dimensionless natural frequency of the linear system. Thus, in considering the general nonhomogeneous problem, it is necessary to be aware of these three dimensionless frequencies:

β_0 - the characteristic, nonlinear frequency,

ω_0 - the natural frequency,

ϕ - the driving frequency.

Either β_0 or ω_0 is an appropriate choice for σ, the non-dimensionalizing frequency. Correspondingly, one would select either a (with β_0)or u (with ω_0) as the base displacement g.

One final rearrangement of equation (9.) is made here to emphasis the characteristic, nonlinear frequency:

(11.) $W''+CW'+\kappa W=\varepsilon f(W)+E\phi^2\exp(i\phi\tau)$

where $\kappa=A+k(1-\Delta/a)+i[-B+\mu k(1-\Delta/a)]$ and

$f(W)=k\Delta(1+i\mu)/\varepsilon[1/|W|-1/a]W$.

Asymptotic expansions may now be introduced to solve equation (11.). The singular method of multiple scales, as described by Nayfeh [6], is appropriate for this problem. The method of averaging gives similar results.

Instead of one time scale τ, assume the problem depends on many time scales:

$$T_0=\tau,\ T_1=\varepsilon\tau,\ T_2=\varepsilon^2\tau,\ldots$$

Henceforth, only T_0 and T_1 are used. Let $W(\tau)=W(T_0,T_1)=W_0(T_0,T_1)+\varepsilon W_1(T_0,T_1)+\ldots$ Equation (11.) becomes a partial differential equation since

$$d/d\tau=(\partial/\partial T_0)(dT_0/d\tau)+(\partial/\partial T_1)(dT_1/d\tau)=D_0+\varepsilon D_1$$

and $(d^2/d\tau^2)=(D_0+\varepsilon D_1)^2$.

Thus, one finds

(12.) $(D_0+\varepsilon D_1)^2(W_0+\varepsilon W_1+\ldots)+C(D_0+\varepsilon D_1)(W_0+\varepsilon W_1+\ldots)$

$+\kappa(W_0+\varepsilon W_1+\ldots)=\varepsilon f(W_0+\varepsilon W_1+\ldots)+E\phi^2\exp(i\phi T_0)$.

Equating like powers of ε yields

(13.) $\varepsilon^0: D_0^2W_0+CD_0W_0+\kappa W_0=E\phi^2\exp(i\phi T_0)$.

This is a linear problem with this steady-state solution

$$W_0=M\exp(i\beta_0T_0)+N\exp(i\phi T_0)$$

where $N=E\phi^2/(-\phi^2+iC\phi+\kappa)$ and $M=M(T_1)$. To determine M one must examine the ε-order problem and chose M to eliminate secular terms; see Nayfeh [6]:

$$\varepsilon^1: \; D_0^2W_1+CW_1+\kappa W_1=-2D_0D_1W_0-CD_1W_0+f(W_0).$$

with $L=k\Delta/\varepsilon$, the right-hand side of the last equation becomes

$$-2i\beta_0M'\exp(i\beta_0T_0)-CM'\exp(i\beta_0T_0)$$

$$+L(1/|W_0|-1/a)[M\exp(i\beta_0T_0)+N\exp(i\phi T_0)]$$

where $|W_0|=\{|M|^2+|N|^2+\bar{M}N\exp[i(\phi-\beta_0)T_0]+M\bar{N}\exp[i(\beta_0-\phi)T_0]\}^{1/2}$

To avoid secular terms one requires that the collective coefficient of $\exp(i\beta_0T_0)$ be zero. Although an analytic solution of the differential equation for $M(T_1)$ has not been found, one can qualitatively assess M based on a similar problem (van der Pol's equation) and specific numerical results (presented in the next section).

Since $M(T_1)$ is complex, it may be written as $M(T_1)=\rho(T_1)\exp[i\hat{\beta}(T_1)]$. Thus,

$W_0=\rho(T_1)\exp[i\beta_0T_0+i\hat{\beta}(T_1)]+N\exp(i\phi T_0)$ or, assuming $\hat{\beta}(T_1)$ is analytic near $t=0$, $W_0=\rho(T_1)\exp[i(\beta_0+\varepsilon\beta_1)\tau+\ldots]+N\exp(i\phi\tau)$. Thus the fundamental frequency of the nonlinear problem is not β_0 but $\beta=\beta_0+\varepsilon\beta_1+\ldots$; however, β must reduce to β_0 when $E\phi^2=0$. This frequency shift can account for the phenomenon of "tracking" that has been observed experimentally [2]. Similarly, the frequency $\gamma=\phi-\beta_0$ that appears in the expression for $|W_0|$ should be considered as $\gamma=\phi-\beta$. Then $1/|W_0|$ shows all frequencies $n\gamma$ and $W_0/|W_0|$ shows all frequencies $n\gamma\pm\beta$, for $n=0,1,\ldots$ This suggest that M has a complex Fourier series of the form

$$\sum_{n=-\infty}^{\infty} s_n \exp(in\gamma T_1).$$

Another factor of M must also be included since numerical examples show that $M\equiv 0$ if $E\phi^2$ is greater than some fixed value. This is similar to the behavior of the van der Pol oscillator; see [6]. Thus, one may speculate that M has a

factor of the form $F=1/[1+\exp(-\eta T_1)]$ where $\eta=\eta(E\phi^2)$. This would imply that $F\to 1$ as $\tau\to\infty$ when $\eta\geq 0$ and $F\to 0$ as $\tau\to\infty$ when $\eta<0$. Thus, M looks like

$$1/[1+\exp(-\eta T_1)] \sum_{n=-\infty}^{\infty} s_n \exp(in\gamma T_1).$$

PSD plots of R show frequencies of $n\gamma$ only while plots of Y show frequencies of ϕ and $n\gamma\pm\beta$.

3. Examples:

Example 1. In this example the system constants used are these: $\mu=0$, $m=1$ lb.-s.^{2}/in., $C_s=240$ lb.-s./in., $K_s=0.$, $K_b=1{,}305{,}000$ lb./in., $Q_s=200{,}000$ lb./in., $\delta=.0000285$ in., and $\omega=500$ Hertz $=1000\pi$ rad./s. Thus, $\beta_0=833.33$ rad./s. and $a=.000060915$ in. The system is made nondimensional using a for the g-displacement and β for the σ-frequency. With these choices, the constants of this equation

$$W''+CW'+[k(1-\Delta/|W|)-iB]W=E\phi^2\exp(i\phi\tau)$$

have these values: $C=.288$, $k=1.8792$, $\Delta=.467865$, $B=.288$, and $\phi=6\pi/5$.

Figures 1 and 2 show changes in the solution Y vs. Z as E assumes the values $100n/(1000\pi)^2a$ for $n=0,1,\ldots,7$. The graphs are plotted for $.2<t\leq .5$s. The initial circle (for E=0) opens into an annular region, which becomes larger and thicker as E increases until a (transition) value of E occurs and the coefficient of $\exp(i\beta\tau)$ becomes zero. Thus, $W=N\exp(i\phi\tau)$, a circle of radius $|N|$. As E increases beyond this transition value, the solution remains a circle (figure 2.d) with radius $|N|=|E\phi^2/(-\phi^2+iC\phi+k(1-\Delta/|N|)-iB|$.

The characteristic, nonlinear frequency β_0 is the angular frequency of the circle when E=0, but this frequency increases as E increases. This tracking phenomenon is displayed in the PSD plots of figures 3 and 4 using the dimensional frequency β. In these figures only the 120-180 Hertz range is shown. At $E=7/10{,}000\pi^2a$, there is no frequency in this range; instead, the circle is tranversed at the forcing frequency, ω.

Figure 5, a typical full PSD plot, is the case $E=4/10{,}000\pi^2 a$. As shown earlier, one expects frequencies of ω and β to appear, as well as harmonics of $n\gamma \pm \beta$ where $\gamma=\omega-\beta$ and $n=1, 2, \ldots$ Thus, with $\beta=150$ Hertz, and $\omega=500$Hertz, one predicts that the PSD plot will exhibit peaks at 150, 200, 500, 550, 850, 900, ... Hertz.

Example 2. In this example, the system constants from CDC[3] are these: $\mu=0$, $m=.20422$ lb.-s.^{2}/in., $C_s=200$ lb.-s./in., $K_s=200{,}000$ lb./in., $K_b=1{,}000{,}000$ lb./in., $\omega=500$ Hertz, $Q_s=C_s\omega/2$ lb./in., and $\delta=.0005$ in. Thus, $\beta=250$ Hertz$=500\pi$rad./s. and $a=.0007183$ in. Figure 6 summarizes changes in Y vs. Z as E varies by $250n/(1000\pi)^2 a$, $n=0,1,\ldots,4$. These graphs are plotted for $.45<t\leq.5$s.

In general, if the time interval is sufficiently large, the plots of annular regions will be completely filled (visually if not mathematically). However, when the ratio of β to γ is p/q for small, positive integers p and q, then the curve actually falls on itself as time evolves and some attractive patterns appear. Figure 6.d is a case where $\beta/\gamma=5/4$, and the picture would look essentially the same whether shown for $.45<t\leq.5$ s. (actual) or for $.45<t\leq50$ s. On the other hand, figure 6.c is more typical and would show a black annulus for $.45<t\leq50$ s.

Example 3. This example uses the same data as example 1, but considers variations in the forcing frequency rather than E; i.e., $E=.7$ and ϕ varies.

For each frequency ϕ one expects to see a plot similar to one of those shown for example 1; thus, at each value of ϕ either a circle or an annulus will describe Y vs. Z. Furthermore, based on continuity considerations, the ϕ-axis will be subdivided into intervals within which each curve is a circle or an annulus.

Example 1 showed that as E increased, the magnitude of the forcing function, $E\phi^2$, increased, and all plots were circles above the transition value of E (and hence $E\phi^2$). A more careful analysis shows that this transition value is based not on the magnitude of the forcing function, but rather on the magnitude of the response at the forcing frequency; i.e., on $E\phi^2/(-\phi^2+i\zeta\phi+\kappa)$. In example 1, ϕ is far

from β_0 and the magnitude of the response is roughly E. But in the present example, one must consider values of ϕ near and far from β_0. For those values near β_0, not only the size of E but also the proximity of ϕ to β_0 will make the magnitude of the response large. Therefore, one may predict that a circle at the forcing frequency will be seen for a plot of Y vs. Z when ϕ is near β, except for very small values of E. Elsewhere, one predicts an annular region unless the value of E is large.

Figures 8 and 9 show the response values Y vs. Z for $.4<t<.5$ s. as ϕ assumes the values .33, .385, .66, .99, 1.10, 1.32, 1.43, 1.65, 2.2, and 3.3 with E held at .7. Here the σ-frequency for nondimensionalizing is ω_0. These irregularly-spaced frequencies were chosen for these reasons:

a. .33 and .385 bound the value of transition from annulus to circle;

b. .66, .99, 1.10 are values close to β;

c. 1.32 and 1.43 bound the value of transition from circle to annulus;

d. 1.65 has a nice picture;

e. 2.20 and 3.30 are limiting values of interest

At another value of E, the pictures would be similar although the transition values would be different. The extreme case E=0 is a circle of radius a with frequency β_0, regardless of ϕ's value. This was shown in figure 1.a.

If a three-dimensional plot Y vs. Z vs. $\phi(=\omega/\omega_0)$ were made for fixed E, one would find a frequency-response plot similar to the usual plots in linear theory. In particular, the maximum value of $(Y^2+Z^2)^{1/2}$ occurs near $\phi=1$. This is shown in figure 8.d where the scale is four times as large as the scale of the other plots. The height of the response curves corresponds to the radius of the steady-state response when the plot is a circle or the outer radius when the plot is an annulus. In general, these response curves will be discontinuous at the transition points.

4. Conclusions:

In studying the Jeffcott rotor with deadband and sinusoidal forcing, one must consider these three frequencies: (a) the forcing frequency ω; (b) the natural frequency, ω_0, of the associated linear problem (deadband $=\delta=0$); and (c) the characteristic, nonlinear frequency β_0. The frequency ω depends only on the forcing function; ω_0 depends only on the system parameters; β, with its base value β_0, depends on both the forcing function and the system parameters.

For a given system and a nonzero, external, sinusoidal force, the y-z response is either a circle at the forcing frequency or an annulus composed of the (major) frequencies β and ω as well as the (minor) harmonic frequencies $n(\omega-\beta)\pm\beta$, for positive integers n.

Frequency-response curves for a nonlinear problem and its associated ($\delta=0$) problem are similar, both reaching a maximum near $\omega=\omega_0$. Each point of the nonlinear plot, however, may represent either the radius of a circle or the outer radius of an annulus. There are also jump discontinuities in the response curves at points of transition between circles and annuli.

Two related problems, which show similar results in preliminary analyses, are rotors with sideforces and rotors with rubbing. Since the analysis of section 2 remains valid if $E\phi^2$ is replaced by one coefficient G, one may consider sideforces as sinusoidals of the form $G\exp(i\omega\tau)$ where $\omega=0$. A rubbing problem may be reduced to a problem with a sideforce if one examines the response in the rotating rather than inertial coordinate system. Both of these problems will be considered more carefully in future work.

The principal obstacle remaining in this analysis is that of finding an explicit expression for transition values; i.e., expressing the transition point from an annulus to a circle as a function of the system and forcing parameters.

This analysis does not allow two or more external forces (e.g., mass imbalance and sideforces). These problems appear to introduce no new theory, but do increase the computational

complications since one must consider not only forcing frequencies ω_1, ω_2 ,..., but also harmonic frequencies $\omega_1+\omega_2$, $\omega_1-\omega_2$, etc.

The addition of asymmetric stiffness introduces difficulties that promise intriguing analyses based on preliminary Runge-Kutta solutions. Not only do the circle/annulus plots become elliptic and occur with their axes rotated with respect to the y, z axes, but there may be other shapes and more than one transition point to consider. These problems, however, greatly extend the model's mimicry of an observed rotor's behavior.

Finally, one needs to cons der stability questions for these nonlinear problems. Superficially, their stabilities are dictated by the corresponding linear problem's stability, but this has not yet been proven.

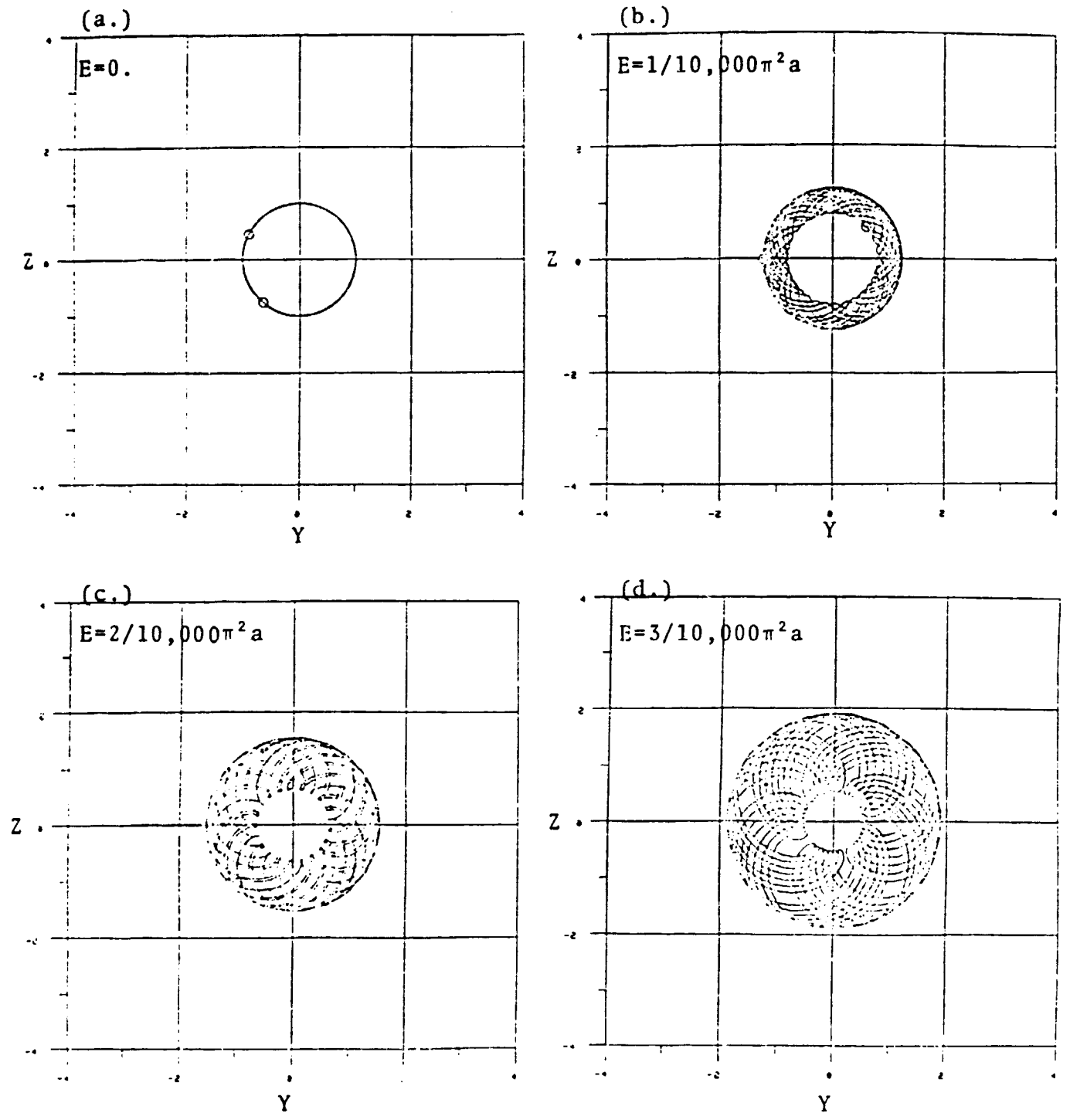

FIGURE 1

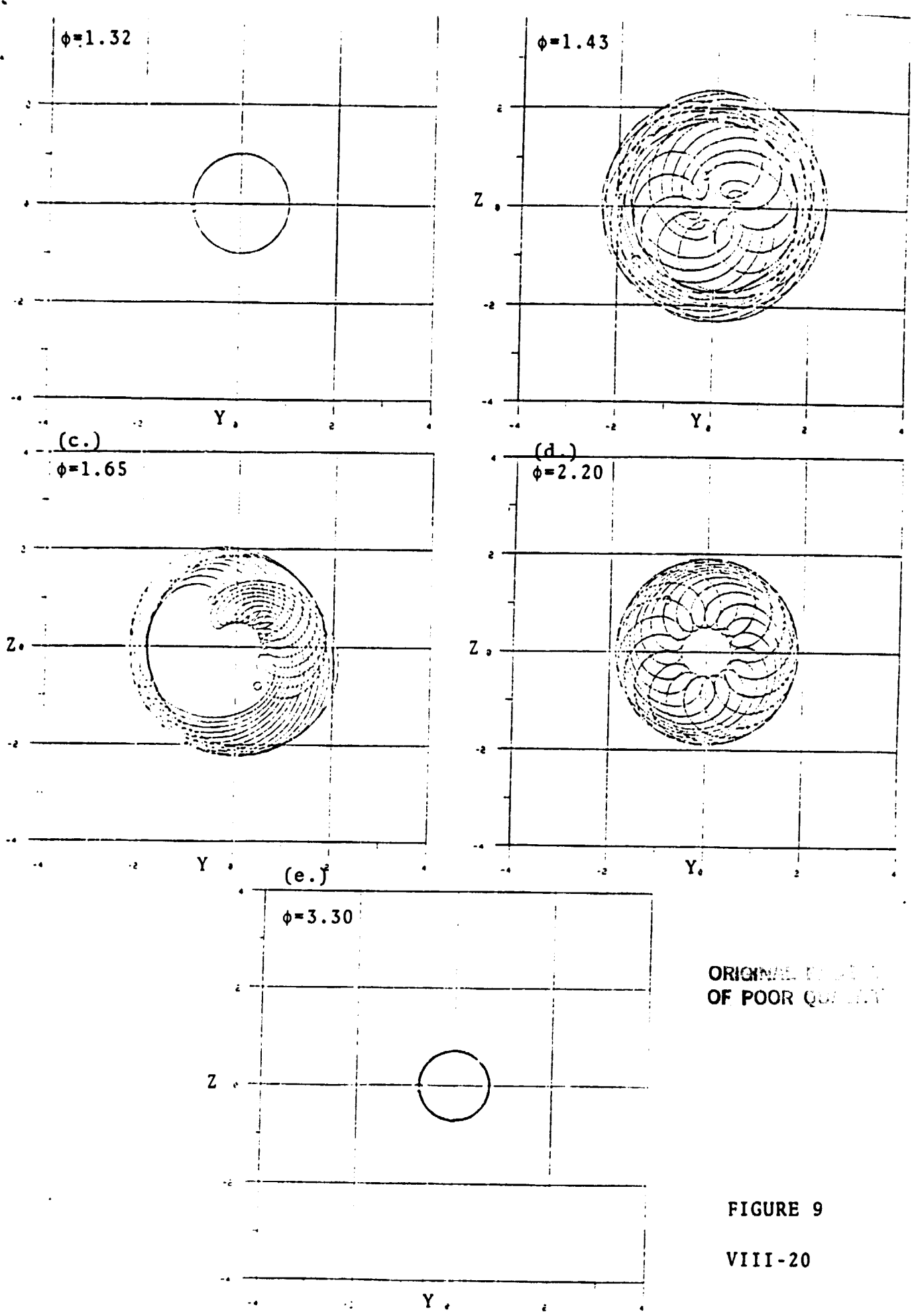

FIGURE 9

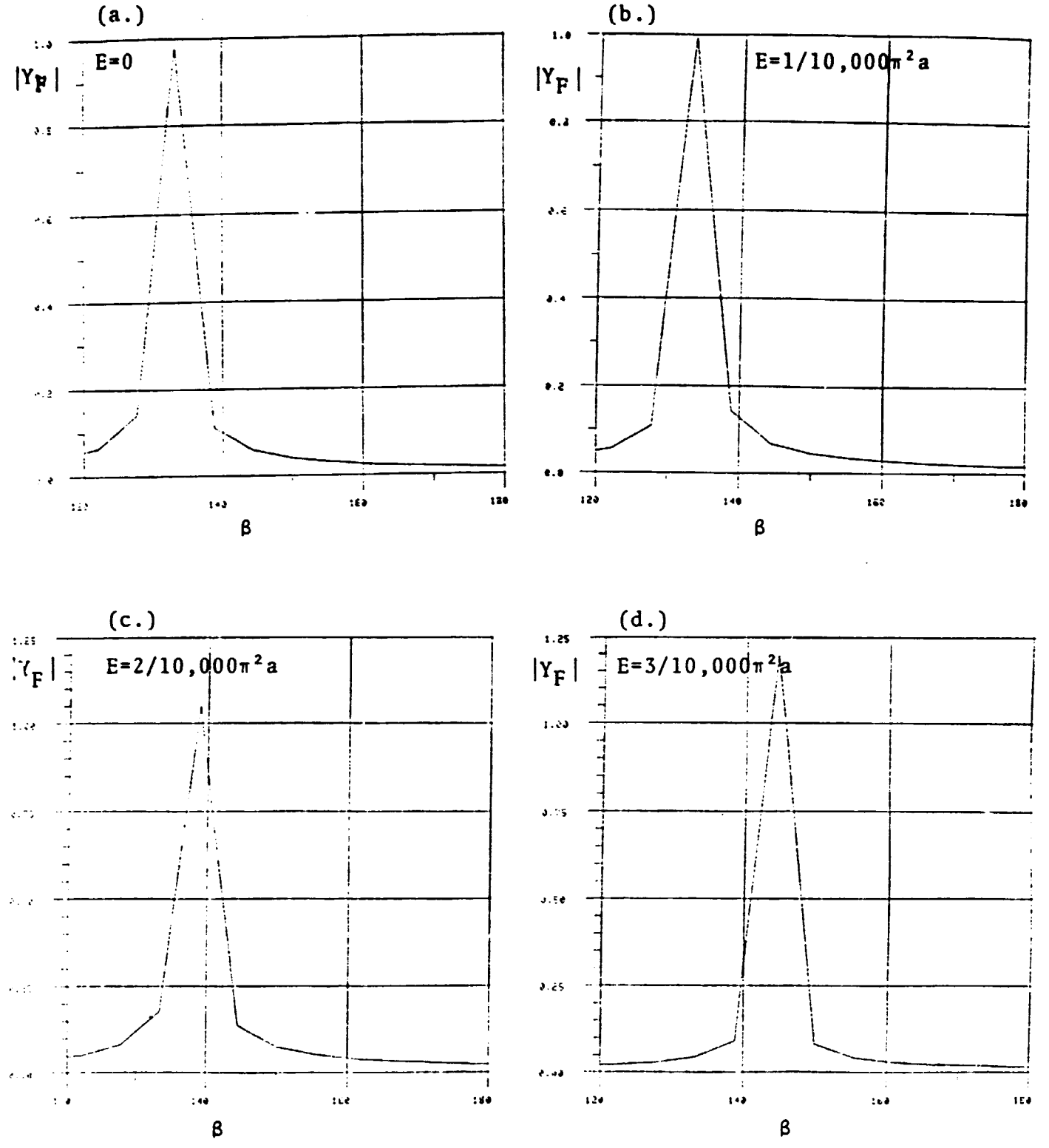

FIGURE 3

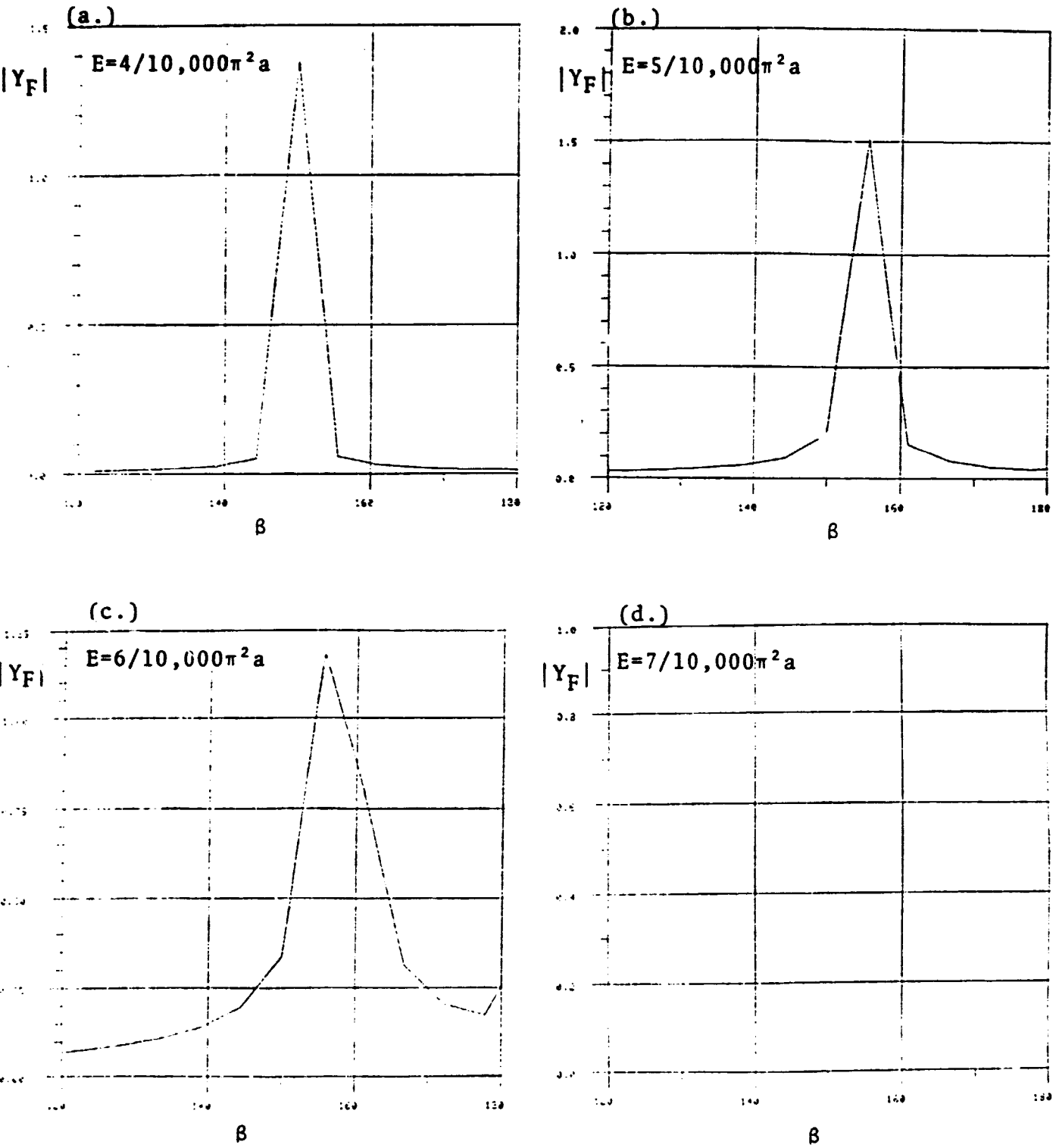

FIGURE 4

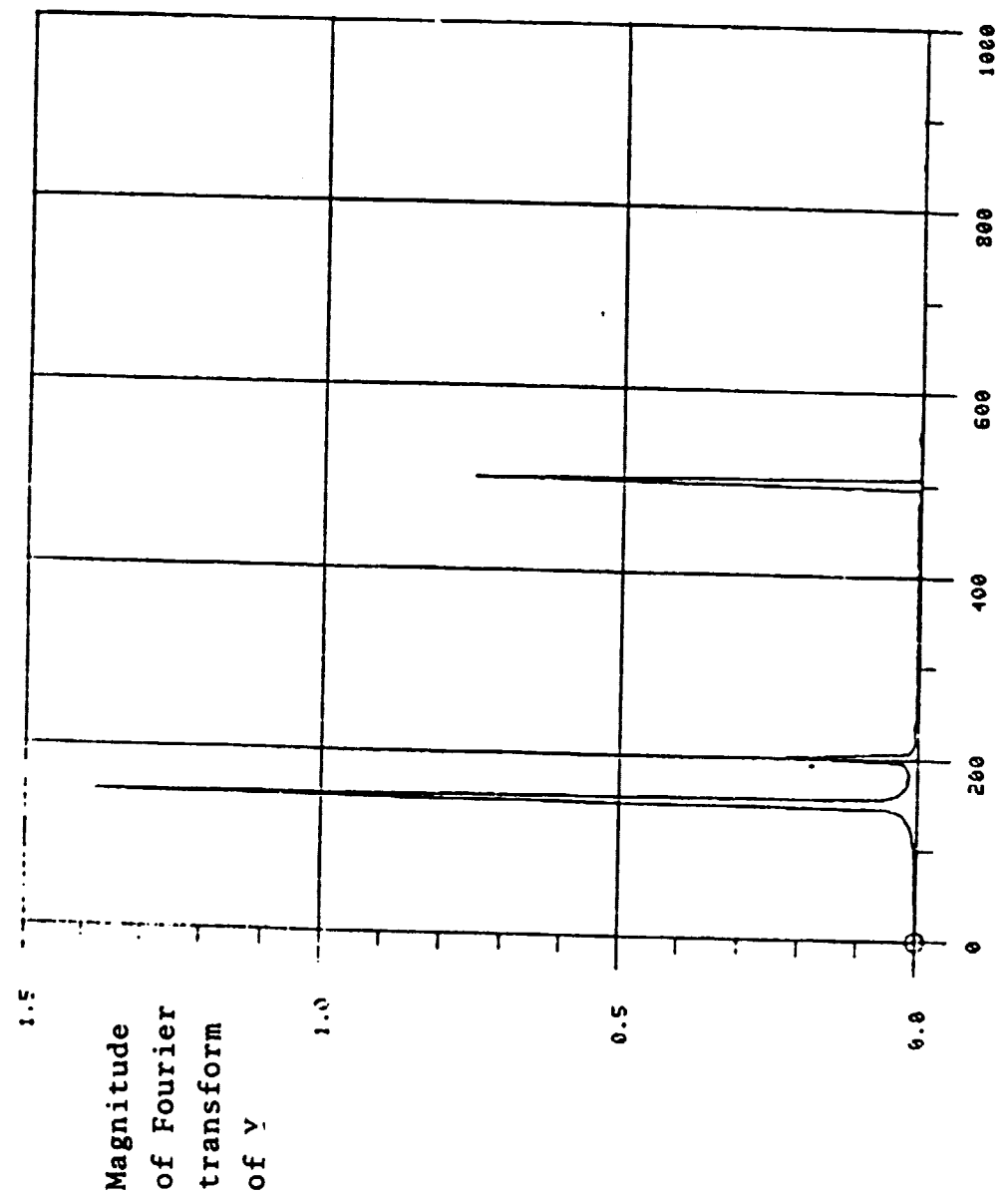

FIGURE 5

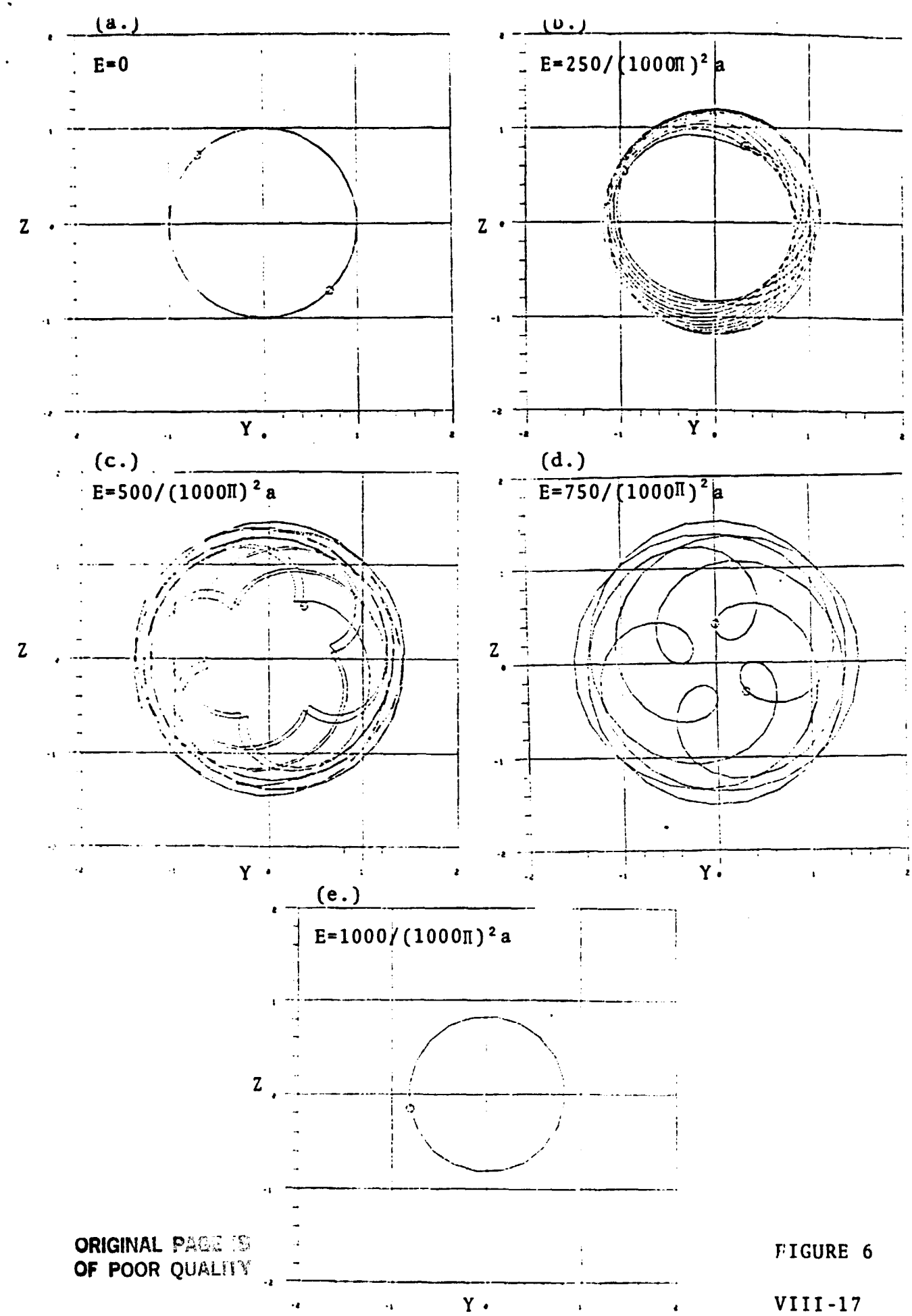

FIGURE 6

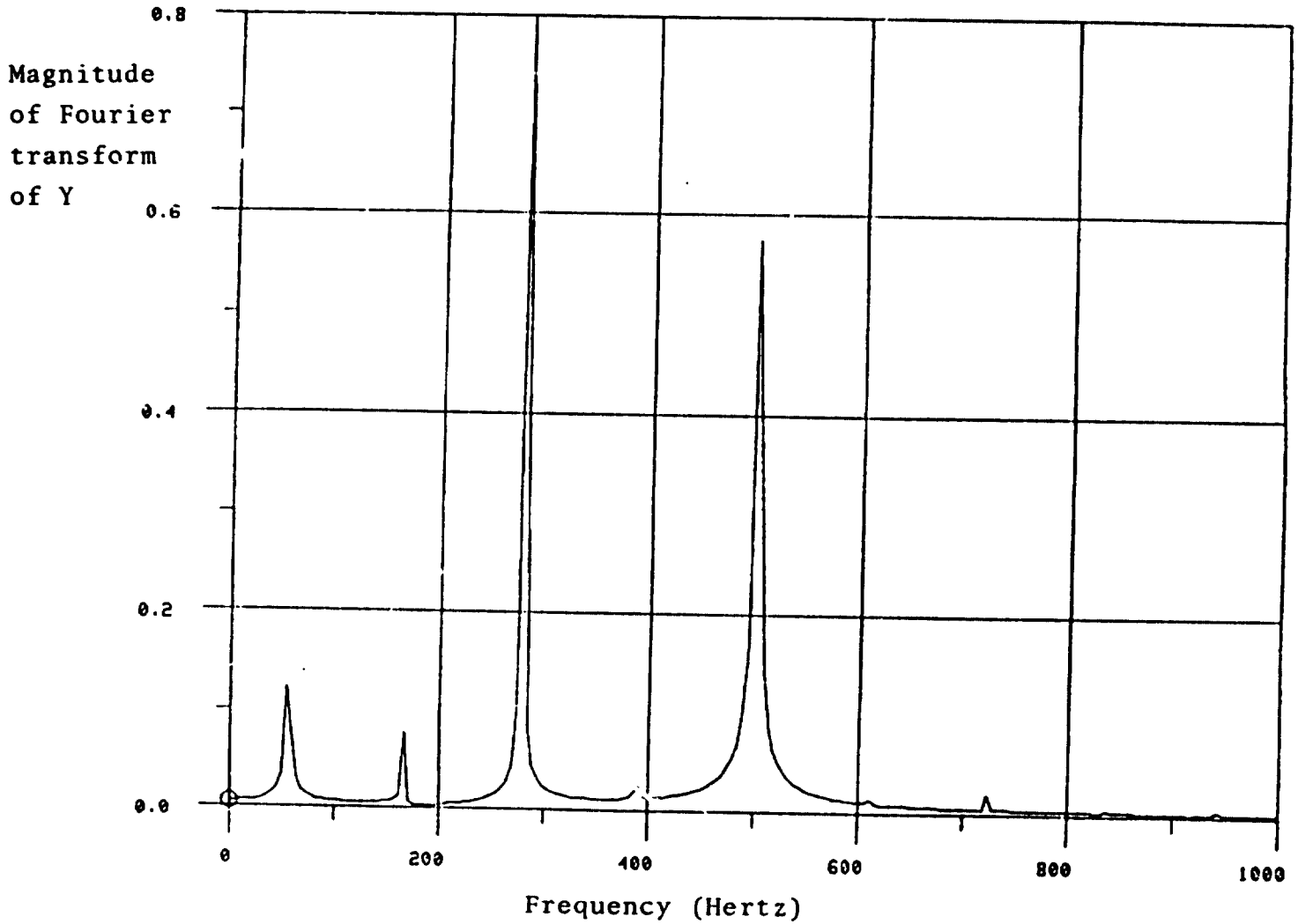

Figure 7

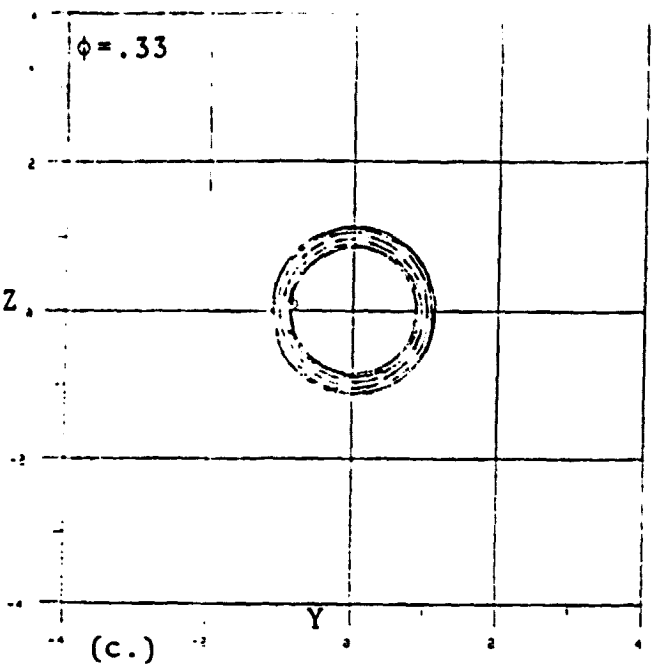

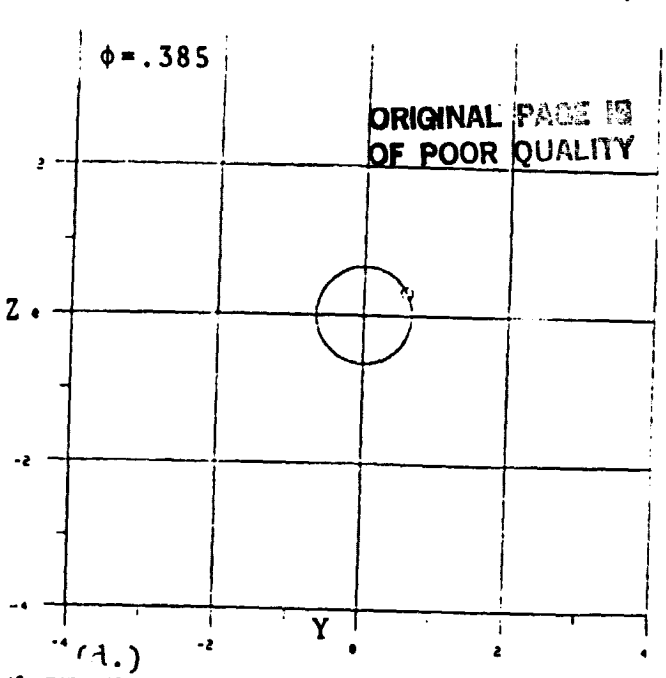

(c.)

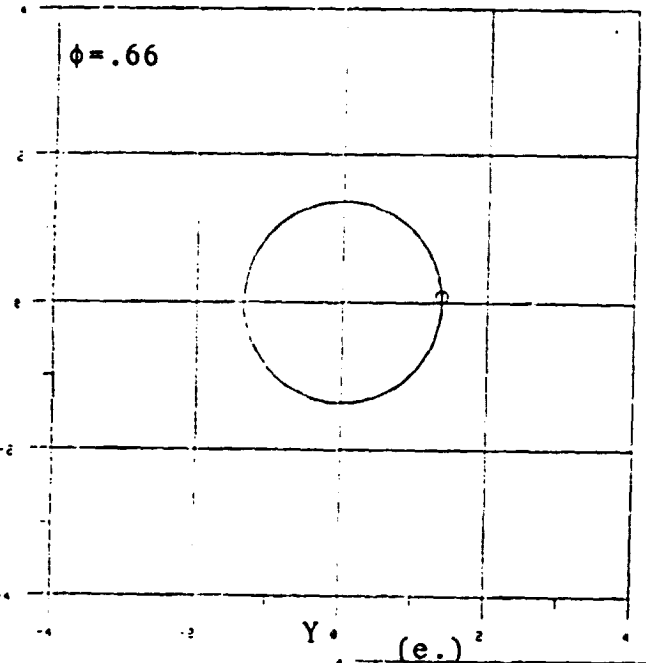

(d.)

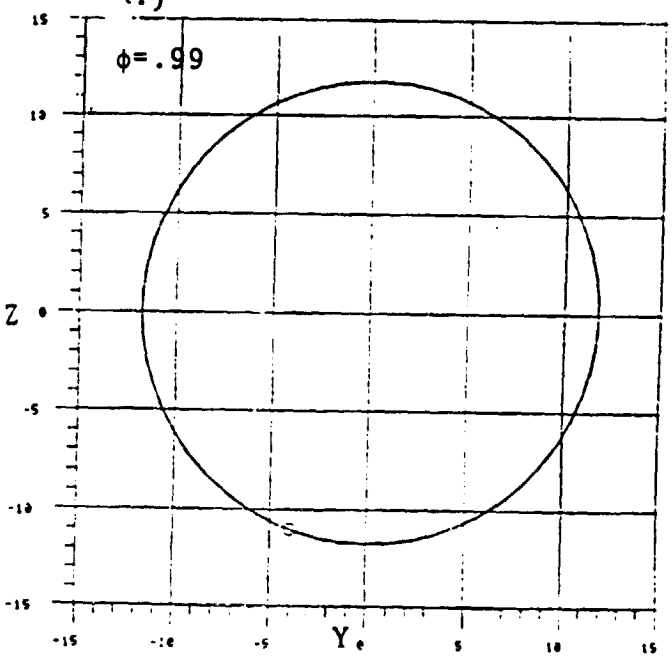

(e.)

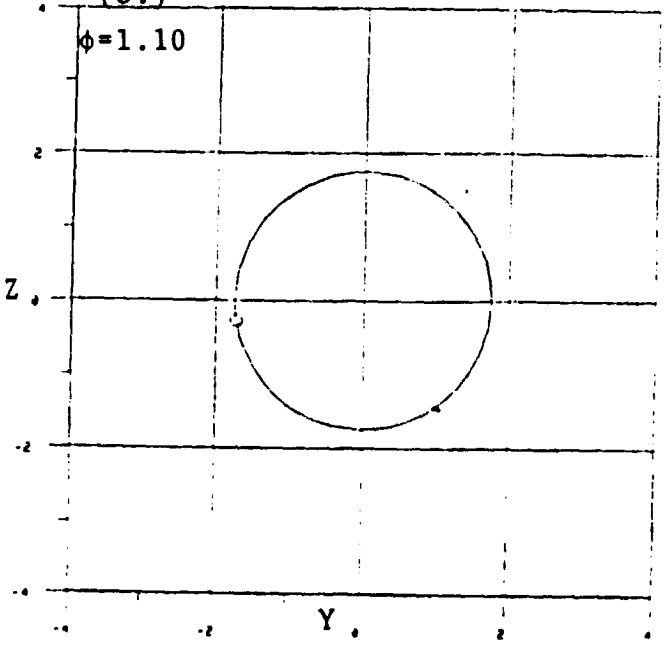

FIGURE 8

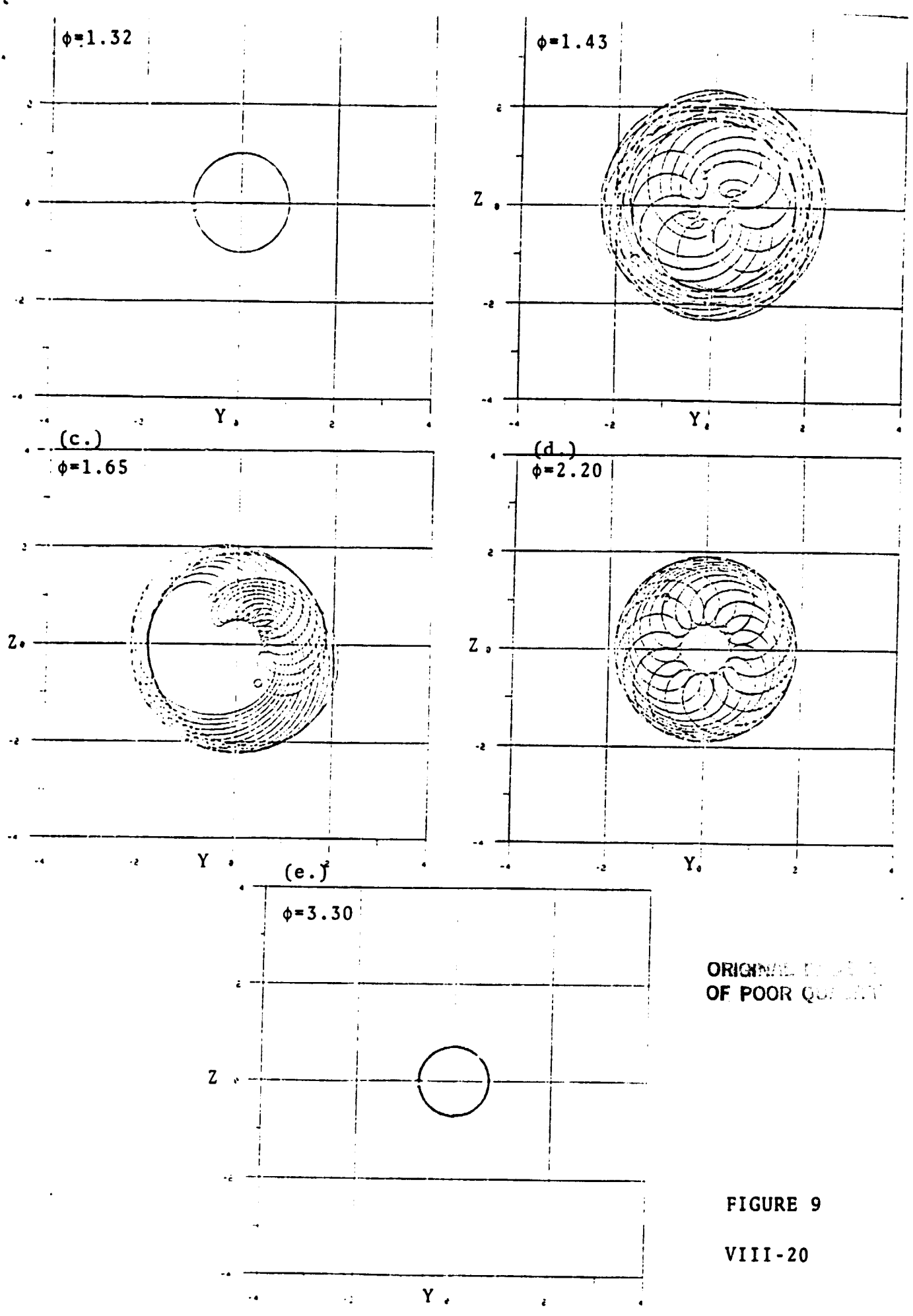

FIGURE 9

5. References:

1. Childs, D. W., "The Space Shuttle Main Engine High-Pressure Fuel Turbopump Rotordynamics Instability Problem", Trans. ASME, Journal of Engineering for Power, Jan. 1978, pp. 48-57.

2. Childs, D. W., "Rotordynamic Characteristics of the HPOTP (High Pressure Oxygen Turbopump) of the SSME (Space Shuttle Main Engine)", NASA MSFC Contract NAS8-34505, Turbomachinery Laboratories Report RD-1-84, 30 January 1984.

3. Control Dynamics Company, "Effects of Bearing Deadbands on Bearing Loads and Rotor Instability", NASA MSFC Contract NAS8-35050, 20 January 1984.

4. Gupta, P. K., Winn, L. W., and Wilcock, D. F., "Vibrational Characteristics of Ball Bearings", Journal of Lubrication Technology, ASME Trans., Vol. 99F, No. 2, 1977, pp. 284-289.

5. Jeffcott, H. H., "The Lateral Vibration of Loaded Shafts in the Neighborhood of a Whirling Speed-The Effect of Want of Balance", Philosophical Magazine, Series 6, Vol. 37, 1919, p. 304.

6. Nayfeh, A. H., Perturbation Methods, J. Wiley & Sons, 1973.

7. Yamamoto, T. T., "On Critical Speeds of a Shaft", Memories of the Faculty of Engineering, Nagoya (Japan) University, Vol. 6, No. 2, 1954.